The influence of high energy electron irradiation on the Schottky barrier height and the Richardson constant of Ni/4H-SiC Schottky diodes

E. Omotoso [a,b,*], W.E. Meyer [a], F.D. Auret [a], A.T. Paradzah [a], M. Diale [a], S.M.M. Coelho [a], P.J. Janse van Rensburg [a]

[a] Department of Physics, University of Pretoria, Private Bag X20, Hatfield 0028, South Africa
[b] Departments of Physics, Obafemi Awolowo University, Ile-Ife 220005, Nigeria

ARTICLE INFO

ABSTRACT

The influence of high energy electron (HEE) irradiation from a Sr-90 radio-nuclide on n-type Ni/4H–SiC samples of doping density 7.1×10^{15} cm^{-3} has been investigated over the temperature range 40–300 K. Current–voltage (I–V), capacitance–voltage (C–V) and deep level transient spectroscopy (DLTS) were used to characterize the devices before and after irradiation at a fluence of 6×10^{14} electrons-cm^{-2}. For both devices, the I–V characteristics were well described by thermionic emission (TE) in the temperature range 120–300 K, but deviated from TE theory at temperature below 120 K. The current flowing through the interface at a bias of 2.0 V from pure thermionic emission to thermionic field emission within the depletion region with the free carrier concentrations of the devices decreased from 7.8×10^{15} to 6.8×10^{15} cm^{-3} after HEE irradiation. The modified Richardson constants were determined from the Gaussian distribution of the barrier height across the contact and found to be 133 and 163 A cm^{-2} K^{-2} for as-deposited and irradiated diodes, respectively. Three new defects with energies 0.22, 0.40 and 0.71 eV appeared after HEE irradiation. Richardson constants were significantly less than the theoretical value which was ascribed to a small active device area.

© 2015 Elsevier Ltd. All rights reserved.

1. Introduction

Metal-semiconductor (MS) Schottky barrier diodes (SBDs) are widely used where diodes with low forward voltage drop, junction capacitance and high switching speed are required [1]. This makes them ideal as rectifiers in photovoltaic systems, high-efficiency power supplies and high frequency oscillators [2]. SBDs also have important uses in optoelectronics, high frequency and bipolar integrated circuits applications [3,4]. The reliability of SBDs is influenced significantly by the quality of the MS junction [5]. The performance of the devices can be quantified experimentally study in terms of their ideality factor, Schottky barrier height (SBH), saturation current, series resistance and free carrier concentration. Among these properties of the MS interface, SBH plays a major role in the successful operation of many devices in transporting electrons across the MS junction [6].

Since room temperature (300 K) measurements of I–V and C–V characteristics alone cannot provide detailed information about the mechanisms responsible for the formation of barrier at the interface of the MS and electrical properties of devices [7], additional insight is gained by characterising the diodes over a wide temperature range (40–300 K). Conclusions may be drawn from the deviation of I–V–T characteristics from the

* Corresponding author at: Department of Physics, University of Pretoria, Private Bag X20, Hatfield 0028, South Africa. Tel.: +274842911287.
E-mail address: ezekiel.omotoso@up.ac.za (E. Omotoso).

ideal thermionic emission current model at lower temperature for many SBDs. The I–V–T characteristics of SBDs based on TE theory reveals an abnormal increase in the ideality factor and a decrease in the SBH with decreasing temperature [8–11]. The abnormal behaviour has been attributed to be a function of the atomic structure, and atomic or barrier inhomogeneities at the MS interface, which are caused by defects, multiple phases and grain boundaries. The barrier inhomogeneities in MS SBDs are often modelled as a Gaussian distribution function and used to provide better understanding to experimental I–V characteristics [12–15].

SiC is a promising semiconductor with a wide bandgap of 3.26 eV [16]. Because of its wide bandgap and chemical stability, it can be used to produce electronic devices that are capable of operating at high temperature, high frequency and high power semiconductor devices, as well as in harsh radiation fields [17–20]. Effects of radiation and temperature on semiconductors are technologically important for radiation to sensing applications, as well as manufacturing processes and high temperature and high power applications [21]. Deep level transient spectroscopy (DLTS) on SBDs is often used to investigate the properties of defects in semiconductors.

Many researchers have reported that some wide bandgap semiconductors such as SiC, ZnO and GaN are radiation hard which makes them suitable for use in harsh radiation environments [18]. Effects of proton, fast electron and fast neutron irradiation on SiC have been investigated by different researchers [18,22–24]. To the best of our knowledge, the effect of high energy electron (HEE) irradiations at fluence of 6×10^{14} cm^{-2} on Ni/4H–SiC has not been reported.

In this work, we present the effect of HEE irradiations on the electrical characteristics of nickel SBDs fabricated on 4H–SiC SBDs measured over wide temperature range (40–300 K). The major aim of this work is to determine the extent to which the characteristics of nickel on n-type 4H–SiC Schottky diodes would be affected by HEE irradiations.

2. Experimental procedure

The samples used for this work were cut from a nitrogen-doped n-type 4H–SiC wafer, polished on both sides with the Si face epi ready, resistivity of 0.02 Ω-cm and doping density of 7.1×10^{15} cm^{-3}. The wafers were supplied by CREE Res. Inc. The samples were cut into smaller pieces with dimension of roughly 2×3 mm^2 and degreased by boiling for 5 min each in trichloroethylene, acetone, methanol and followed by 1 min rinse in de-ionized water. They were etched in 40% hydrogen fluoride for 30 s in order to remove the native oxide layer on the samples, then rinsed in de-ionized water, followed by blow drying with nitrogen gas prior to thermally fabrication of nickel ohmic contact on the back surface (1.0×10^{18} cm^{-3} doped side) of the samples. Resistive evaporation was employed for the fabrication of nickel ohmic and Schottky contacts because it is known to neither introduce defects nor contaminate the samples. The ohmic contact with a thickness of 3000 Å was deposited at a rate of 0.4 Å s^{-1}. For ohmic contact formation, the

samples were annealed in a tube furnace under flowing argon gas at 950 °C for 10 min to form nickel silicides [25].

Before deposition of the Schottky contact, the samples were cleaned in an ultrasonic water bath for 3 min each in trichloroethylene, acetone and methanol, followed by 1 min rinsed in de-ionized H$_2$O after the annealing of the ohmic contact. Nickel Schottky contacts were resistively evaporated through a metal contact mask and had an area of 2.4×10^{-3} cm^2 and a thickness of 1000 Å deposited at a rate of 0.2 Å s^{-1} under a vacuum of approximately 10^{-5} Torr.

The sample was irradiated through the Schottky contacts by HEE from a strontium-90 radioactive source at a fluence rate of 7×10^9 electrons-cm^{-2} s^{-1}. The irradiation was carried out at room temperature and lasted for 24 h, which resulted in a fluence of 6×10^{14} electrons-cm^{-2}. The energy distribution of electron emitted by strontium-90 radionuclide has been reported by Auret *et al.* [26].The sample was characterized at room temperature and in the dark using I–V and C–V station, consisting of a HP 4140 B pA metre/DC voltage source and HP 4192 A LF Impedance Analyser, respectively. Hereafter, the sample was placed in a closed cycle helium cryostat and characterised by conventional DLTS, I–V–T and C–V–T measurements in wide temperature range. This procedure was performed before and after HEE irradiation.

3. Results and discussion

3.1. C–V characteristics

The fabricated devices were subjected to irradiation at room temperature. Both as-deposited and irradiated devices were examined by the C–V method at different temperatures. Fig. 1 shows the plot of capacitance as a function of reverse bias voltage. The capacitance decreased with a decrease in temperature. The capacitance increased with decreasing reverse voltage for both, but the capacitance after irradiation was lower, as also be reported [27,28]. The C^{-2} (pF^{-2}) as a function of reverse bias voltage, V (V) before and after HEE irradiation measured at 1 MHz with the samples at temperatures range
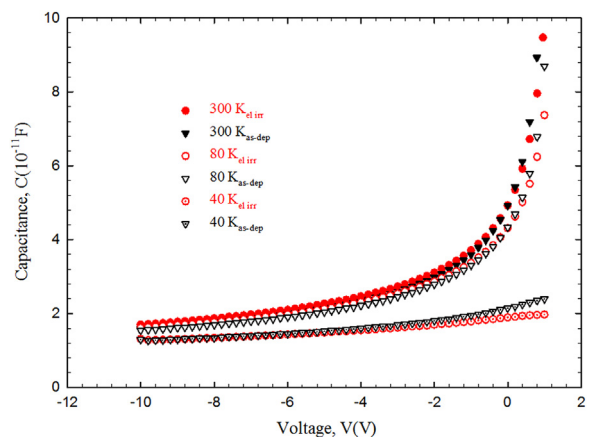

Fig. 1. The C–V characteristics of Schottky barrier diodes of Ni/n-4H–SiC before and electron irradiation in temperature range 40–300 K.
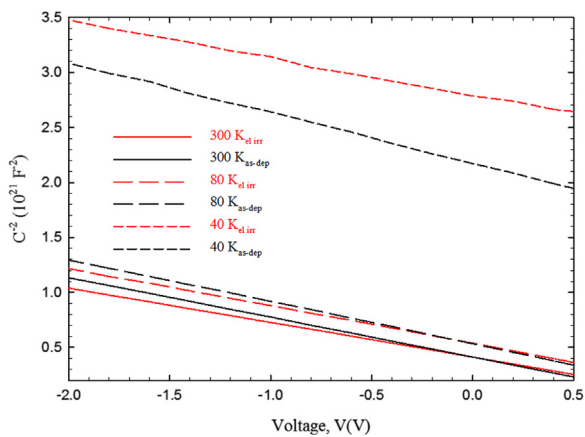
40–300 K are depicted in Fig. 2. The result obtained showed a good SBDs for both devices. There was no abrupt degradation between the as-deposited and irradiated devices at temperature range 80–300 K. The $C–V$ characteristics changed more rapidly with temperature, and the difference between the as-deposited and the irradiated diodes became more pronounced below 80 K. The slope of plot C^{-2} versus V is approximately constant for the temperature range 80–300 K for both samples which indicates that all the dopant is ionized due to the presence of the electric field [29]. The plot in Fig. 2 is deduced from Eq. (1) which represents the depletion layer in Schottky diodes. The N_t, V_{bi} and $\phi_{C–V}$ were determined from the plot and tabulated in Table 1. The free carrier concentrations, N_t decreased with irradiation and temperature which is as a result of the defects introduced from the HEE irradiation into the SiC.

$$\frac{1}{C^2} = \frac{2(V_o - V_{bi})}{q\varepsilon_s A^2 N_t} \qquad (1)$$

where q is the charge, ε_s is the permittivity of semiconductor, A is the effective area of the diode, and V_o can be obtained from the intercept of reverse voltage when C^{-2} is equal to zero. The zero-bias barrier heights for both devices were determined from Eq. (2).

$$\phi_{C-V} = V_{bi} + \frac{kT}{q}\ln\frac{N_c}{N_t} \qquad (2)$$

From Fig. 2, the free carrier concentrations of the sample were determined from the slope of the plots according to Eq. (1). The free carrier removal rate, ŋ can be obtained

Fig. 2. Graph of C^{-2} as a function of applied voltage characteristic of SBDs of Ni/4H–SiC before and after electron irradiation in temperature range 40–300 K.

from Eq. (3) below

$$\eta = \frac{\Delta(N_D - N_A)}{\varphi} \qquad (3)$$

where $\Delta(N_D - N_A)$ is the change in free carrier concentration before and after HEE irradiation, φ is the fluence at which the sample was bombarded [30]. At room temperature (300 K), the change in free carrier concentration from 7.8×10^{15} (before irradiation) to 6.8×10^{15} cm^{-3} (after HEE irradiation) is 1.0×10^{15} cm^{-3} and the fluence received by the sample was 6.0×10^{14} cm^{-2}. The free carrier removal rate was calculated as 1.67 cm^{-1} for irradiation of the sample with energy 546 keV from Sr-90 radionuclide. The value of ŋ calculated here is approximately 4670 times lower than that of SiC bombarded by 5.4 MeV alpha-particles [31]. The HEE irradiation has less impact on the electrical properties of Ni/4 H–SiC than alpha-particle irradiation [31].

3.2. I–V characteristics

The forward semi-log $I–V$ characteristics of the Ni/4H–SiC SBD measured at temperature range 40–300 K before and after electron irradiation are shown in Fig. 3 in order to know the temperature effects on the deep energy levels. The plots show linearity up to a current of approximately 1×10^{-4} A for as-deposited and irradiated devices except at lower temperatures (80 K below). It can be observed that $I–V$ plots show lower current with lower temperature. This is in accord with the equation describing current transport across a SBD by thermionic emission–diffusion theory [32,33].

The effect of irradiation on the Ni/4H–SiC diode as well as temperature can be quantified in terms of the ideality factor (n), Schottky barrier height ($\phi_{I–V}$), saturation current (I_s) and series resistance (R_s) obtained from the $I–V$ plots. Measurements on the Schottky contacts were taken before and after the devices were irradiated. Table 1 compares the properties of the samples. The effective Richardson constant for both samples were obtained from the Eq. (4). Schottky barrier heights of the contacts were determined from the $I–V$ characteristics analysed by using the thermionic emission model [5,32,33].

$$I_s = AA^*\exp(-\frac{q\phi_{I-V}}{kT}) \qquad (4)$$

where A^* is the effective Richardson constant, $\phi_{I–V}$ is the effective SBH at zero bias, k is the Boltzmann constant and T is absolute temperature in Kelvin.

It could be deduced from Table 1 that the SBH$_{I–V}$ decrease and the ideality factor increase, with decreasing in

Table 1
Comparison of some electrical parameters of Ni/n-type 4H–SiC before and after electron irradiation estimated from $I–V$ and $C–V$ characteristics at 40 and 300 K.

Samples	n	I_s (A)	R_s (Ω)	V_{bi} (V)	N_t (cm^{-3})	ϕ_{I-V} (eV)	ϕ_{C-V} (eV)
As–deposited(300 K)	1.04	1.5×10^{-20}	48	1.07	7.8×10^{15}	1.44	1.36
As-deposited (40 K)	4.02	2.0×10^{-44}	664	5.03	5.9×10^{15}	0.37	5.06
24h electron irradiation (300 K)	1.13	1.4×10^{-19}	60	1.32	6.8×10^{15}	1.38	1.60
24h electron irradiation (40 K)	4.14	1.4×10^{-45}	1684	7.92	5.2×10^{15}	0.36	7.95

temperature [33–37]. It was also observed that SBHs$_{I-V}$ decrease and the ideality factors increase after HEE irradiation which corroborated what has earlier reported [23,24], but was in contrast with what was observed by Lin *et al.* [38].

From Eq. (4), ϕ_{I-V} is given as

$$\phi_{I-V} = \frac{kT}{q} \ln\left(\frac{AA^*T^2}{I_s}\right) \qquad (5)$$

Comparing the SBH for *I–V* and *C–V* measurements, it was observed experimentally that SBHs' do not agree. The SBH increased after irradiation for both *I–V* and *C–V*, but to greater extent for *C–V* measurements. This is in agreement with what has been reported in literature [39–43]. The causes for a difference in this parameters are deep impurity levels, surface inhomogeneity, quantum mechanical tunnelling, interfacial layer and states, image force lowering, and edge leakage currents [44].

Fig. 4 shows a gradual change in ideality factor and SBH before and after HEE irradiation for SBD from temperatures above 120 K. It can also be deduced from the plot that there was sporadic deviation of electrical behaviours of SBD from thermionic emission theory at lower
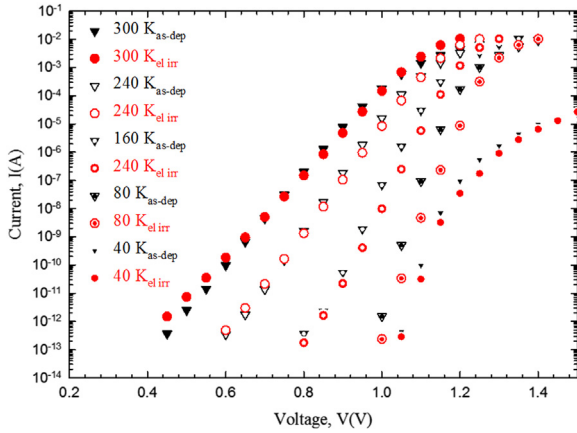
temperatures (below 120 K). Generation-recombination was dominant at temperatures below 80 K. Ideality factor and SBH of the Ni/4H–SiC had strong reciprocal temperature dependence at lower temperatures. It was also observed earlier for alpha-particle irradiated devices [31]. These deviations are due to the presence of inhomogeneities at the interface (such as surface defects and inhomogeneity in doping concentration) [20,33–37,45–47]. There was little noticeable change in the ideality factors and SBH at temperature 120 K and above, for before and after irradiation.

3.3. The Richardson plot

Fig. 5 shows the Richardson's plot of ln (I_s/T^2) as a function of $1/T$ for as-deposited and HEE irradiated samples. The temperature dependent behaviour of *n* and SBH predicted an inhomogeneous barrier height and deviation from thermionic emission and diffusion theory as shown in Fig. 4 [20,34,37,47]. Barrier height can be determined in another way by re-writing Eq. (6) as Eq. (9) below

$$\ln\left(I_s/T^2\right) = \ln AA^* - q/k\phi_{I-V}.1/T \qquad (6)$$

The diode showed very high dependence of ideality factor on temperature, which led to the distortion of the plot from linearity. The plots were linearized by multiplying *ln* (I_s/T^2) by *n* as suggested by Schroder [48]. The experimental values of A^* before and after irradiation were estimated from the intercept of the plot to be 4.1×10^{-8} and 2.8×10^{-12} A cm^{-2} K^{-2}, respectively. The values were extremely small compared to the theoretical value of effective Richardson constant of 146 A cm^{-2} K^{-2} [34,36,37,49,50], which indicate that the active area was smaller than the device area [47], and the effect of barrier inhomogeneity [8]. The mean barrier heights for both were deduced from the slope of the insert plot in Fig. 5 to be 1.41 and 1.30 eV. It has been reported earlier by many researchers that the deviation of the Richardson constants from theoretical value may be as a result of the effect of the barrier inhomogeneity at the MS interface and some other factors such as crystal defects and potential

Fig. 3. The current versus voltage characteristics of Ni/4H–SiC before and after irradiation measured in temperature range 40–300 K.
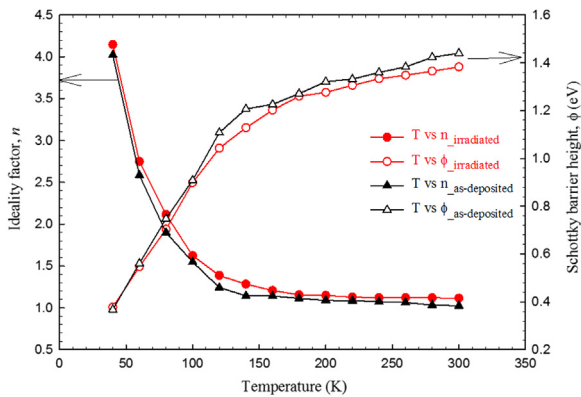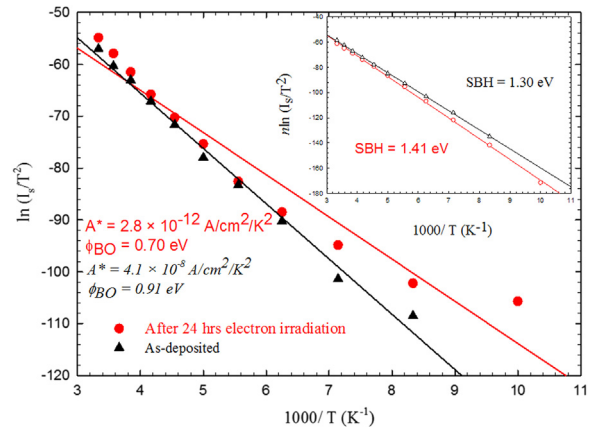

Fig. 4. Ideality factors and Schottky barrier heights as function of temperature before and after irradiation, measured in temperature range 40–300 K.

Fig. 5. The Richardson plot, ln(I_s/T^2) versus 1000/T for Ni/4H–SiC before and after irradiation in the temperature range 40–300 K. The inset shows the plot of $n[\ln(I_s/T^2)]$ versus 1000/T.

fluctuation [8,31,34,47]. Since the deviation cannot be explained by the thermionic emission diffusion model, the Gaussian distribution model of barrier height has been used.

3.4. The modified Richardson plot

The Gaussian distribution model has been used to correct the deviation that cannot be explained with thermionic emission diffusion (TED) which occurred as a result of barrier height inhomogeneities. The abnormal deviation from TE theory has been suggested by some researchers [12,20,33–37,46,47,51] that the distribution barrier heights is a Gaussian distribution $P(\phi_B)$ with mean value of SBH ($\overline{\phi}_B$) and standard deviation as shown in Eq. (7) [10, 13, 32, 52–54].

$$P(\phi_B) = \frac{1}{\sigma_s \sqrt{2\pi}} \exp\left(-\frac{\left(\phi_B - \overline{\phi}_B\right)^2}{2\sigma^2{}_s}\right) \tag{7}$$

where $1/\sigma_s\sqrt{2\pi}$ is the normalisation constant of the Gaussian barrier height distribution. The total current, I (V) across the MS of the SBD containing barrier inhomogeneities that can be expressed in integral form in Eq. (8) [12, 13, 55].

$$I(V) = \int_{-\infty}^{\infty} I(\phi_B, V) P(\phi_B) d\phi_B \tag{8}$$

where $P(\phi_B)$ is the normalised distribution function that gives probability of accuracy of barrier height, and $I(\phi_B, V)$ is the current, at a bias for barrier height based on the ideal TED theory. The expressions for GD of apparent barrier height, ϕ_{ap} at zero bias [10,11,56–59] and apparent ideality

factor, n_{ap} [57] are derived from Eq. (4) to be Eqs. (9) and (10) as shown below

$$\phi_{ap} = \overline{\phi}_{BO}(T=0) - \frac{q\sigma^2{}_{so}}{kT} \tag{9}$$

$$\frac{1}{n_{ap}} - 1 = \rho_2 - \frac{q\rho_3}{2kT} \tag{10}$$

where $\overline{\phi}_B(T=0)$ is the mean barrier height at zero bias and was determined from the intercept of Fig. 6 to be 1.64 and 1.63 eV for as-deposited and after HEE irradiation, respectively, and σ_{so} are standard deviation at zero bias (were determined from the slope of Fig. 6 to be 0.113 eV and 0.104 eV) and ρ_2 and ρ_3 are the voltage coefficients which may be temperature dependent [34,36] and they were obtained from the intercept of the insert of Fig. 6 to be -8.9×10^{-2} and -8.0×10^{-3} (for as-deposited), and -6.4×10^{-2} and -5.1×10^{-3} (after HEE irradiation). The results are tabulated in Table 2. It can be assumed from the results obtained that the $\overline{\phi}_B$ and σ_s are linearly bias dependent on the parameters of Gaussian ($\overline{\phi}_B = \overline{\phi}_{BO} + \rho_2 V$ and $\sigma_s = \sigma_{s0} + \rho_3 V$) and quantifying the voltage deformation of Schottky barrier height distribution [10,11,54]. It was observed that the existence of a Gaussian distribution caused a decrease in zero bias barrier height. The extent of deviation was determined by the standard deviation which is generally significant at low temperature.

The deviation between experimental and theoretical values of the Richardson constants was described by a modified Richardson plot. The modified Richardson constant was obtained by combining Eq. (5) with Eq. (6).

$$\ln\left(\frac{I_s}{T^2}\right) - \left(\frac{q^2\sigma^2}{2k^2T^2}\right) = \ln(AA^{**}) - \frac{q\phi_{Bm}}{kT} \tag{11}$$
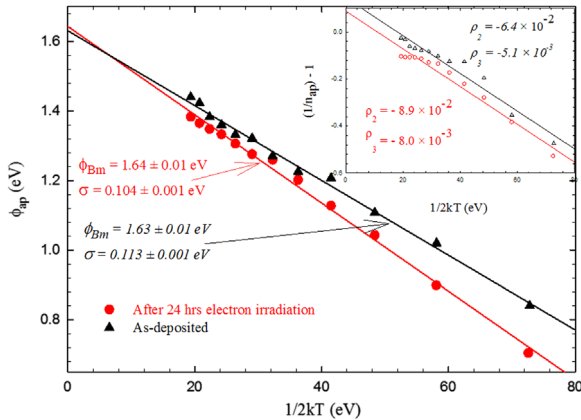
Fig. 6. The zero bias apparent barrier height versus 1/2kT for Ni/4H–SiC before and after irradiation. The insert shows the plot of $(1/n_{ap})$–1 versus 1/2kT.
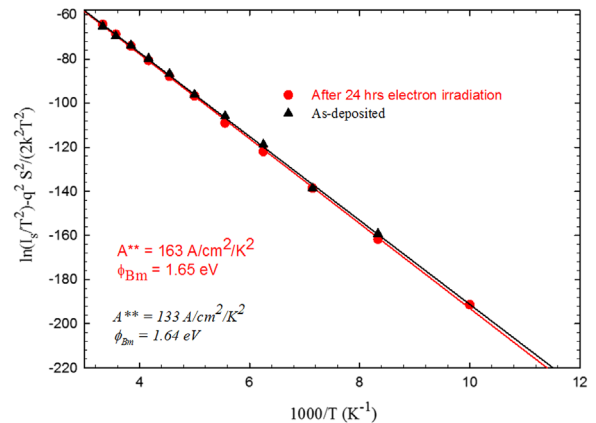
Fig. 7. The modified Richardson plot for Ni/4H-SiC Schottky diode before and after electron irradiation at temperature range 40-300 K.

Table 2
The characteristics of SBDs of 4 H–SiC before and HEE irradiation.

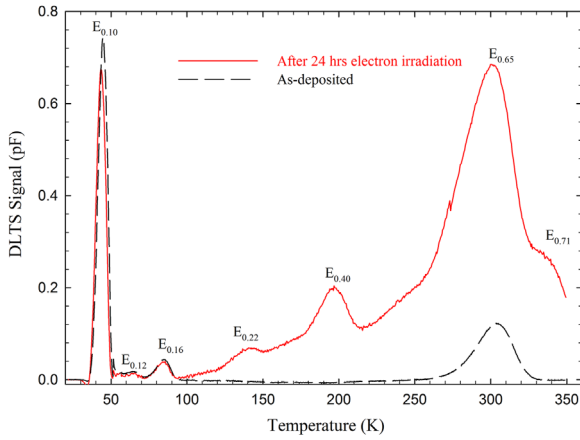| Samples	ρ_2 ($\times 10^{-2}$)	ρ_3 ($\times 10^{-3}$)	σ_{so} (eV) ± 0.001	$\overline{\phi}_{BO}(T=0)$ (eV) ± 0.01	$\overline{\phi}_B$(eV) ± 0.01	A^* (A cm^{-2} K^{-2})	A^{**} (A cm^{-2} K^{-2})
As-deposited	−6.4	−5.1	0.113	1.63	1.64	4.1×10^{-8}	133
After electron irradiation	−8.9	−8.0	0.104	1.64	1.65	2.8×10^{-12}	163

Fig. 8. DLTS spectra for the Ni/4H–SiC before and after electron irradiation. The temperature range 52–350 K scaled up by factor 10.
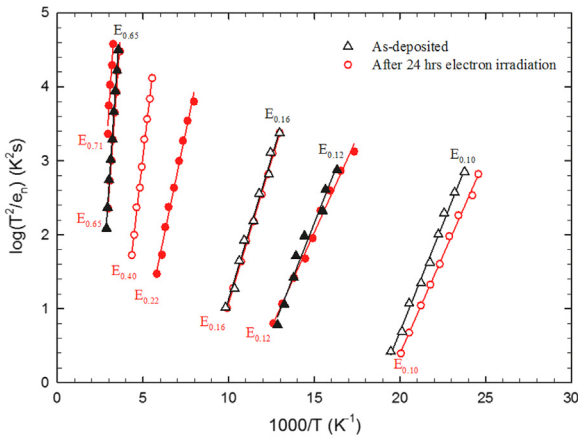

Fig. 9. The Arrhenius plots for the DLTS of as–deposited and after irradiation Ni/4H–SiC.

Fig. 7 shows the plot of $\ln(I_s/T^2) - (q^2\sigma^2/2k^2T^2)$ as function of $1000/T$. The mean $\overline{\phi}_{BO}$ was determined directly from the slope of the plot to be 1.64 ± 0.01 eV and 1.65 ± 0.01 eV for as-deposited and irradiated devices, respectively. The zero mean barrier height obtained was much closer to those obtained from the plot ϕ_{ap} versus $1/2kT$ in Fig. 6. The modified Richardson constants, A^{**} before and after HEE irradiation was determined from the intercept of the straight line to be 133 and 163 A cm^{-2} K^{-2}, respectively. The values were in good agreement with the theoretical value of 146 A cm^{-2} K^{-2} [49,60], though higher due to spatially inhomogeneous SBHs [20]. The modified Richardson constant obtained was in line with what has been observed during the alpha-particle irradiation [31]. The values of $\overline{\phi}_{BO}$ and A^{**} for as-deposited and irradiated devices showed the extent at which Ni/4H–SiC SBDs could be affected by HEE irradiation at the aforementioned fluence. From these results, we concluded that the HEE irradiation did not influence the mean barrier height, but did influence modified Richardson constant. The same conclusion has been drawn for alpha-particle irradiated 4H–SiC SBDs [31].

3.5. Deep level transient spectroscopy (DLTS)

Fig. 8 shows the DLTS spectra for the samples before and after HEE irradiation. Fig. 9 shows the Arrhenius plots. The measurements were obtained at temperatures range 22–350 K, at a quiescent reverse bias of -5.0 V, filling pulse amplitude of 6.0 V, filling pulse width of 2.0 ms and a rate window of 20 s^{-1}. The sample before irradiation revealed four defects with levels labelled as $E_{0.10}$, $E_{0.12}$, $E_{0.16}$ and $E_{0.65}$ and their corresponding apparent capture cross sections were 3×10^{-11} cm^2, 1×10^{-15} cm^2, 1×10^{-15} cm^2 and 4×10^{-15} cm^2, respectively. The sample after irradiation revealed seven defects with energy levels labelled as $E_{0.10}$, $E_{0.12}$, $E_{0.16}$, $E_{0.22}$, $E_{0.40}$, $E_{0.65}$ and $E_{0.71}$, and their corresponding apparent capture cross sections were 1×10^{-16} cm^2, 4×10^{-12} cm^2, 1×10^{-15} cm^2, 2×10^{-17} cm^2, 3×10^{-15} cm^2, 3×10^{-15} cm^2 and 3×10^{-15} cm^2. Some of these defects were confirmed from the literature [61]. Three new defects ($E_{0.22}$, $E_{0.40}$ and $E_{0.71}$) were introduced after the sample was irradiated by HEE. The formation of new defects caused changes in the I–V and C–V characteristics and the parameters of the Schottky barrier diodes.

4. Conclusions

The Ni/4 H–SiC Schottky contacts were successfully fabricated by resistive evaporation. The I–V and C–V measurements at 300 K before and after fluence of 6×10^{14} electrons-cm^{-2} irradiation revealed good Schottky contacts which alone did not provide satisfactory results. From the forward I–V measurements, n, SBH, R_s increased with irradiation but I_s decreased with irradiation measured at 300 K. The reverse currents were significantly constant within the range of our system. C–V measurements revealed a decrease in free carrier concentration. The effects of high energy electron irradiations on Ni/4H–SiC SBD was also investigated using I–V, C–V and DLTS, measured in a wide temperature range 40–300 K. For the temperature range 80–300 K, thermionic emission was the dominant transport mechanism. Generation-recombination proved to be dominant at temperatures below 80 K. The ideality factor and SBH of the devices had strong reciprocal temperature dependence at lower temperature. The modified Richardson constants before and after HEE irradiation were 133 and 163 A cm^{-2} K^{-2}, respectively, by using Gaussian distribution method. The values of A^{**} were in good agreement with the theoretical value. We concluded that HEE irradiation of fluence 6×10^{14} electrons-cm^{-2} did not influence the mean barrier height, but did influence modified Richardson constant. The removal rate of approximately 1.67 cm^{-1} was calculated which corroborate the use of SiC in radiation harsh environments.

generated by the NRF supported are that of authors and that NRF accepts no liability whatsoever in this regard.

References

[1] R.L. Van Tuyl, C.A. Liechti, IEEE J. Solid-State Circuits 9 (1974) 269–276.

[2] A. Elasser, M.H. Kheraluwala, M. Ghezzo, R.L. Steigerwald, N.A. Evers, J. Kretchmer, T.P. Chow, IEEE Trans. Ind. Appl. 39 (2003) 915–921.

[3] S. Takayuki, U. Tsuneo, S. Seizo, M. Yoshihiko, Jpn J.Appl. Physics 19 (1980) 459.

[4] A.F. Özdemir, A. Turut, A. Kökçe, Semicond. Sci. Technol. 21 (2006) 298.

[5] E. Rhoderick, R. Williams, Oxford Science, Oxford, 1988.

[6] V. Janardhanam, A. Ashok Kumar, V. Rajagopal Reddy, P. Narasimha Reddy, J. Alloy. Compd. 485 (2009) 467–472.

[7] S. Zeyrek, M.M. Bulbul, S. Altindal, M.C. Baykul, H. Yuzer, Braz. J. Phys. 38 (2008) 591–597.

[8] İ. Dökme, Ş. Altindal, M.M. Bülbül, Appl. Surf. Sci. 252 (2006) 7749–7754.

[9] Ş. Karataş, Ş. Altindal, M. Çakar, Phys. B: Condens. Matter 357 (2005) 386–397.

[10] S. Zhu, R.L. Van Meirhaeghe, C. Detavernier, F. Cardon, G.P. Ru, X.P. Qu, B.Z. Li, Solid-State Electron. 44 (2000) 663–671.

[11] A. Gümüş, A. Türüt, N. Yalçin, J. Appl. Phys. 91 (2002) 245–250.

[12] J.H. Werner, H.H. Güttler, J. Appl. Phys. 69 (1991) 1522–1533.

[13] C. Subhash, Semicond. Sci. Technol. 19 (2004) 82.

[14] Y.P. Song, R.L. Van Meirhaeghe, W.H. Laflère, F. Cardon, Solid State Electron. 29 (1986) 633–638.

[15] P.G. McCafferty, A. Sellai, P. Dawson, H. Elabd, Solid-State Electron. 39 (1996) 583–592.

[16] L.M. Tolbert, B. Ozpineci, S.K. Islam, M.S. Chinthavali, Power and Energy Syst. Proc. 1 (2003) 317–321.

[17] V. Kazukauskas, J.-V. Vaitkus, Opto-Electron. Rev. 12 (2004) 377–382.

[18] J. Grant, W. Cunningham, A. Blue, V. O'Shea, J. Vaitkus, E. Gaubas, M. Rahman, Nucl. Instrum. Methods Phys. Res. A: Accel. Spectrom. Detect. Assoc. Equip. 546 (2005) 213–217.

[19] M.C. Driver, R.H. Hopkins, C.D. Brandt, D.L. Barrett, A.A. Burk, R.C. Clarke, G.W. Eldridge, H.M. Hobgood, J.P. McHugh, P.G. McMullin, R.R. Siergiej, S. Sriram, Gallium Arsenide Integrated Circuit (GaAs IC), in: Proceedings of the 15th Annual Symposium on Technical Digest, 1993, pp. 19–21.

[20] V. Kumar, A.S. Maan, J. Akhtar, J. Vac. Sci. amp; Technol. B 32 (2014) 041203.

[21] A. Akbay, H. Korkut, K. Ejderha, T. Korkut, A. Türüt, J. Radioanal. Nucl. Chem. 289 (2011) 145–148.

[22] K. Çınar, C. Coşkun, Ş. Aydoğan, H. Asıl, E. Gür, Nucl. Instrum. Methods Phys. Res. B: Beam Interact. Mater. Atoms 268 (2010) 616–621.

[23] K. Çınar, C. Coşkun, E. Gür, Ş. Aydoğan, Nucl. Instrum. Methods Phys. Res. B: Beam Interact. Mater. Atoms 267 (2009) 87–90.

[24] J. Benkovska, L. Stuchlikova, D. Buc, L. Čaplovic, Phys. Status Solidi (a) 209 (2012) 1384–1389.

[25] T. Marinova, A. Kakanakova-Georgieva, V. Krastev, R. Kakanakov, M. Neshev, L. Kassamakova, O. Noblanc, C. Arnodo, S. Cassette, C. Brylinski, B. Pecz, G. Radnoczi, G. Vincze, Mater. Sci. Eng.: B 46 (1997) 223–226.

[26] F.D. Auret, S.A. Goodman, G. Myburg, W.O. Barnard, D.T.L. Jones, J. Appl. Phys. 74 (1993) 4339–4342.

[27] S. Ashok, J.M. Borrego, R.J. Gutmann, J. Appl. Phys. 51 (1980) 1076–1084.

[28] F. Roccaforte, S. Libertino, F. Giannazzo, C. Bongiorno, F. La Via, V. Raineri, J. Appl. Phys. 97 (2005).

[29] C. Raynaud, K. Isoird, M. Lazar, C.M. Johnson, N. Wright, J. Appl. Phys. 91 (2002) 9841–9847.

[30] F. Auret, S. Goodman, M. Hayes, M. Legodi, H. Van Laarhoven, D.C. Look, Appl. Phys. Lett. 79 (2001) 3074–3076.

[31] E. Omotoso, W.E. Meyer, F.D. Auret, A.P. Paradzah, M. Diale, S.M.M. Coelho, P.J. Janse Van Rensberg, Nucl. Instr. Meth. Phys. Res. B, submitted for publication, 2015.

[32] S.M. Sze, K.K. Ng, Physics Semiconductor Devices, John Wiley & Sons, New York, 2006.

[33] M.E. Aydın, N. Yıldırım, A. Türüt, J. Appl. Phys. 102 (2007) 043701.

[34] Z. Ouennoughi, S. Toumi, R. Weiss, Phys. B: Condens. Matter 456 (2015) 176–181.

[35] M. Gülnahar, Superlattices Microstruct. 76 (2014) 394–412.

[36] S. Alialy, Ş. Altındal, E.E. Tanrıkulu, D.E. Yıldız, J. Appl. Phys. 116 (2014) 083709.

[37] S. Shankar Naik, V. Rajagopal Reddy, Superlattices Microstruct. 48 (2010) 330–342.

[38] Z. Lin, Z. Yi-Men, Z. Yu-Ming, H. Chao, M. Yong-Ji, Chin. Phys. B 18 (2009) 1931.

[39] E. Hökelek, G.Y. Robinson, Appl. Phys. Lett. 40 (1982) 426–428.

[40] C.R. Crowell, V.L. Rideout, Solid-State Electron. 12 (1969) 89–105.

[41] M. Soylu, B. Abay, Microelectron. Eng. 86 (2009) 88–95.

[42] M. Soylu, F. Yakuphanoglu, J. Alloy. Compd. 506 (2010) 418–422.

[43] C. Coskun, N. Gedik, E. Balcı, Semicond. Sci. Technol. 21 (2006) 1656.

[44] C.R. Crowell, Solid-State Electron. 20 (1977) 171–175.

[45] R.R. Ciechonski, Device Characteristics of Sublimation Grown 44H–SiCLayers, Linkping Univ., Linkping, 2005.

[46] L. Huang, F. Qin, S. Li, D. Wang, Appl. Phys. Lett. 103 (2013) 033520.

[47] S. Toumi, A. Ferhat-Hamida, L. Boussouar, A. Sellai, Z. Ouennoughi, H. Ryssel, Microelectron. Eng. 86 (2009) 303–309.

[48] D.K. Schroder, A John Willey & Sons, inc., 3rd ed. 2006.

[49] A. Itoh, T. Kimoto, H. Matsunami, Electron Device Lett. IEEE 16 (1995) 280–282.

[50] F. Roccaforte, F. La Via, A. Baeri, V. Raineri, L. Calcagno, F. Mangano, J. Appl. Phys. 96 (2004) 4313–4318.

[51] J.H. Werner, H.H. Güttler, J. Appl. Phys. 73 (1993) 1315–1319.

[52] M.K. Hudait, P. Venkateswarlu, S.B. Krupanidhi, Solid-State Electron. 45 (2001) 133–141.

[53] S. Zhu, R.L. Van Meirhaeghe, C. Detavernier, G.P. Ru, B.Z. Li, F. Cardon, Solid State Commun. 112 (1999) 611–615.

[54] S. Zeyrek, Ş. Altındal, H. Yüzer, M.M. Bülbül, Appl. Surf. Sci. 252 (2006) 2999–3010.

[55] P.M. Gammon, A. Pérez-Tomás, V.A. Shah, O. Vavasour, E. Donchev, J.S. Pang, M. Myronov, C.A. Fisher, M.R. Jennings, D.R. Leadley, P.A. Mawby, J. Appl. Phys. 114 (2013) 223704.

[56] Y.P. Song, R.L. Van Meirhaeghe, W.H. Laflère, F. Cardon, Solid-State Electron. 29 (1986) 633–638.

[57] S. Chand, S. Bala, Appl. Surf. Sci. 252 (2005) 358–363.

[58] E. Özavcı, S. Demirezen, U. Aydemir, Ş. Altındal, Sens. Actuat. A: Phys. 194 (2013) 259–268.

[59] H. Tecimer, S. Aksu, H. Uslu, Y. Atasoy, E. Bacaksız, Ş. Altındal, Sens. Actuat. A: Phys. 185 (2012) 73–81.

[60] F. Roccaforte, C. Bongiorno, F. La Via, V. Raineri, Appl. Phys. Lett. 85 (2004) 6152.

[61] V.V. Kozlovskiĭ, V.V. Emtsev, K.V. Emtsev, N.B. Strokan, A.M. Ivanov, V.N. Lomasov, G.A. Oganesyan, A.A. Lebedev, Semiconductors 42 (2008) 242–247.